



## RESEARCH ARTICLE

# Biomimetic sponges improve functional muscle recovery following composite trauma

Andrew Dunn<sup>1</sup> | Gabriel Haas<sup>1</sup> | Joshua Madsen<sup>1</sup> | Natalia Ziemkiewicz<sup>1</sup> |  
Jeffrey Au<sup>1</sup> | David Johnson<sup>1</sup> | Charles West<sup>1</sup> | Hannah Chauvin<sup>1</sup> |  
Sara McBride Gagy<sup>2</sup>  | Koyal Garg<sup>1</sup> 

<sup>1</sup>Department of Biomedical Engineering, Parks College of Engineering, Aviation, and Technology, Saint Louis University, St. Louis, Missouri, USA

<sup>2</sup>Department of Orthopedic Surgery, Saint Louis University, Saint Louis, Missouri, USA

## Correspondence

Koyal Garg, Department of Biomedical Engineering, Parks College of Engineering, Aviation, and Technology, 3507 Lindell Blvd, St. Louis, MO 63103, USA.  
Email: [koyal.garg@slu.edu](mailto:koyal.garg@slu.edu)

## Funding information

National Institute of General Medical Sciences, Grant/Award Number: 1R15GM129731

## Abstract

There is a dearth of therapies that are safe and effective for the treatment of volumetric muscle loss (VML), defined as the surgical or traumatic loss of muscle tissue, resulting in functional impairment. To address this gap in orthopedic care, we developed a porous sponge-like scaffold composed of extracellular matrix (ECM) proteins (e.g., gelatin, collagen, and laminin-111) and an immunosuppressant drug, FK-506. While the majority of VML injuries occur in orthopedic trauma cases, pre-clinical models typically study muscle injuries in isolation without a concomitant bone fracture. The goal of this study was to investigate the extent to which FK506 loaded biomimetic sponges support functional muscle regeneration and fracture healing in a composite trauma model involving VML injury to the tibialis anterior muscle and osteotomy (OST) to the tibia. In this model, implantation of the FK-506 loaded biomimetic sponges limited the extent of inflammation while increasing the total number of myofibers, mean myofiber cross-sectional area, myosin-to-collagen ratio, and peak isometric torque compared to untreated VML+OST muscles on Day 28. Although all tibia fractures were bridged by Day 28 post-injury, fracture healing was impaired in response to an adjacent VML injury. Sponge treatment increased bone callus volume, yet the bridged mineralized bone volume was not significantly different. Taken together, these results suggest that biomimetic sponges primarily benefitted muscle repair and may provide a promising therapy for traumatized muscle.

## KEYWORDS

bone, muscle, repair, tissue engineering, trauma

## 1 | INTRODUCTION

Musculoskeletal injuries are common in both military and civilian populations. In the United States, 65.8 million musculoskeletal injuries required medical attention in 2011, accounting for ~77% of total injuries<sup>1</sup> with treatment costs estimated to be ~\$176

billion annually. Fractures were the most common type (~26%) of musculoskeletal injuries requiring medical treatment in the year 2010.<sup>2</sup> Open fractures account for roughly 3% of fractures each year (~150,000/year in the United States).<sup>3</sup> The debridement of necrotic or infected soft tissue surrounding the fracture either causes or exacerbates volumetric muscle loss (VML). VML is

defined as the traumatic or surgical loss of muscle tissue with resultant functional impairment. Bone fracture coupled with an adjacent VML injury greatly compromises the recovery of the affected limb.<sup>4-6</sup>

Clinically, the emphasis of treating musculoskeletal trauma is on bone repair. Orthopedic surgeons have a variety of options for fracture fixation and bone grafting.<sup>7,8</sup> However, clinical options for VML repair are limited. Current standard of care for VML involves physical therapy,<sup>9</sup> bracing, or autologous muscle flaps.<sup>10,11</sup> While these treatments may reduce early complications and strengthen the remaining muscle mass, they do not support regeneration of the lost muscle. As a result, unsuccessful treatment of orthopedic trauma involving VML may contribute to limb amputation, long-term disability, loss of productivity, substantial medical costs, and lower quality of life.<sup>12</sup> Our previous work has shown that patients with type III open tibia fractures that undergo successful bone healing have persistent muscle-related disability due to VML.<sup>4</sup>

In the clinic, injury classification and healing outcomes after open fractures are dependent on the extent of surrounding soft tissue trauma, highlighting the role of soft tissue-derived components in fracture healing.<sup>13</sup> Preclinical models of fracture with concomitant VML consistently show decreased or delayed repair at the fracture site.<sup>14</sup> Intact muscle is known to support bone healing through mechanical, cellular, trophic, and vascular mechanisms.<sup>15,16</sup> Studies have shown that if porous membranes are placed between muscle and bone, fracture healing is improved only when the pores are large enough to allow diffusion of growth factors and peptides.<sup>17,18</sup> Moreover, the selective blockade of bone contact with fasciocutaneous tissues resulted in normal fracture healing while the prevention of muscle-bone contact markedly compromised bone repair.<sup>17</sup> This result occurred despite a greater vascularity in the fasciocutaneous tissue at all-time points, suggesting that exchange of cellular and soluble mediators between muscle and bone is essential for successful fracture repair.

It has been shown that heightened and prolonged immune response to composite muscle-bone trauma impairs both muscle and bone regeneration.<sup>14</sup> We found that injecting FK-506, an FDA-approved immunosuppressant, into rats with composite muscle-bone trauma significantly reduced infiltration of innate and adaptive immune cells in the VML defect, but it did not regenerate functional muscle.<sup>6</sup> We have previously demonstrated that biomimetic sponges composed of extracellular matrix (ECM) proteins (e.g., gelatin, collagen, and LM-111) can stimulate myogenic regeneration in a murine model of VML injury (~10% defect).<sup>19</sup>

In this study, the VML injury in the rat tibialis anterior (TA) muscle (~20% defect) is further challenged with an adjacent tibia osteotomy (OST). Using this model of composite muscle-bone trauma, we investigate the extent to which FK-506 loaded biomimetic sponges can support functional muscle regeneration and fracture healing. We hypothesize that a combination of regenerative ECM proteins and immunomodulatory agent will improve tissue regeneration in a composite trauma model.

## 2 | MATERIALS AND METHODS

### 2.1 | Preparation of FK-506 loaded biomimetic sponges

Biomimetic sponges were fabricated as reported previously.<sup>20</sup> Briefly, a porcine skin gelatin (3 wt%; Sigma-Aldrich) was combined with 1-ethyl-3-(3-dimethylaminopropyl) (EDC) carbodiimide hydrochloride (20 mM; Thermo Fisher Scientific) and rat tail collagen I (3 mg/ml; Gibco) at a 70:30 gelatin: collagen ratio. Laminin (LM)-111 (50 µg/ml; Trevigen) and FK506 (25 µM; Abcam) were added to the solution and aliquoted into 48-well plates at 700 µl/well. The solution was allowed to gel and was subjected to slow freezing for 48 h before lyophilization. Before implantation, the sponges were disinfected with ethanol for 5 min, rinsed twice with sterile phosphate-buffered saline (PBS) and incubated in sterile PBS overnight.

### 2.2 | Animal model

This study was conducted in compliance with the Animal Welfare Act, the implementing Animal Welfare Regulations, and in accordance with the principles of the Guide for the Care and Use of Laboratory Animals. All animal procedures were approved by the Saint Louis University's Institutional Animal Care and Use Committee (protocol number: 2645).

Male Lewis rats (10–12 weeks old; Charles Laboratory) were housed in a vivarium accredited by the Association for Assessment and Accreditation of Laboratory Animal Care International and provided with food and water ad libitum. Following 1 week of acclimatization, the animals were anesthetized via 2.5% isoflurane with oxygen and injected subcutaneously with Buprenorphine SR (1 mg/kg) and randomly assigned to the following experimental groups ( $n = 5-8$ /group): untreated OST, treated OST, untreated VML+OST, and treated VML+OST. Age-matched cage controls ( $n = 4-6$ /time-point) were used for comparison as uninjured muscles. The surgical site was aseptically prepared, and a lateral incision was made through the skin to reveal the tibia. An OST was performed with a piezoelectric saw (Acteon) 5 mm distal from the tibial crest. A 0.76 mm x 3 cm unthreaded Kirschner pin (K-pin) was driven through the tibial plateau to the medullary canal to fix the fractured bone. The subset receiving FK-506 loaded sponge treatment has a 3 mm diameter sponge disk placed between the proximal and distal ends of the fracture before the K-pin was driven through the defect site.

To create the VML injury, the TA muscle was isolated from the surrounding musculature. A metal plate was inserted behind the muscle, and a 6 mm punch biopsy created a full thickness defect (~20%) in the belly of the muscle. The biopsy was removed and weighed for consistency. A 6 mm diameter FK-506 loaded sponge disk was implanted in the muscle defect in the subset receiving sponge treatment. Bleeding was controlled with light pressure, and the skin incision was closed with skin staples. Bilateral procedures were performed on individual animals. Injury type and treatment was

the same in both legs. Animals recovered for 7, 14, or 28 days before being euthanized under deep anesthesia by exsanguination followed by cervical dislocation. Radiographs of fractured hindlimbs were obtained at 1-, 7-, 14-, and 28-day post-injury to verify pin placement and fracture fixation. Animals with pin slips were excluded from the study. As per veterinarian's recommendation, the subset of animals that received VML+OST and OST-only injuries and were euthanized at the Day 28 time-point, were also injected with enrofloxacin (5 mg/kg) 1 day before surgery, immediately after surgery, and for 5 days post-surgery.

Body mass and TA muscle mass were recorded at euthanasia. Animals were identified using a number code and investigators were blinded to group allocation. From both injured hindlimbs, the upper half of the TA muscle was frozen in liquid nitrogen chilled 2-methylbutane (Thermo Fisher Scientific) while the lower half of the muscle was snap frozen in liquid nitrogen, before being stored at  $-80^{\circ}\text{C}$ . Tibia from one hindlimb was wrapped in sterile saline-soaked gauze and stored frozen at  $-80^{\circ}\text{C}$  for gene expression or micro-computed tomography (microCT) analysis, while the other was stored in 10% formalin at  $4^{\circ}\text{C}$  for histological analysis.

### 2.3 | Serum analysis

At the time of euthanasia, whole blood (5–10 ml) was collected through cardiac puncture under anesthesia. The blood sample was allowed to clot for ~30 min followed by centrifugation at 1000g for 10 min at  $4^{\circ}\text{C}$ . Supernatant containing serum was analyzed using Luminex magnetic bead multiplex enzyme-linked immunosorbent assays (ELISA) as per manufacturer's protocols (EMD Millipore) to quantify interleukin (IL)-2 levels from  $n = 3-5$  animals per group.

### 2.4 | Histology

Frozen muscle cross-sections (15  $\mu\text{m}$ ) were stained with hematoxylin and eosin (H&E), collagen 1 (1:100; ab34710; Abcam), sarcomeric myosin (1:50; MF20; Developmental Studies Hybridoma Bank), laminin (1:100; ab11575; Abcam), CD68 (1:50; MCA341R; AbD Serotec), nuclei (DAPI; 1:100; Invitrogen), CD3 (1:100; ab5690; Abcam), CD31 (1:100; R&D systems), and  $\alpha$ -bungarotoxin (1:100; Invitrogen). Appropriate fluorochrome-conjugated secondary antibodies (1:100; Invitrogen) were used as described previously.<sup>21-23</sup>

Full-slide muscle sections ( $n = 5-8$  muscles/group) stained with myosin heavy chain (MHC) and collagen (COL) were used to quantify the MHC:COL ratio by % area as described previously.<sup>20</sup> Full-slide laminin stained sections ( $n = 4-8$  muscles/group) were used to define individual myofiber cross-sectional area (CSA) through analysis in a MATLAB program.<sup>20</sup>

Tibiae were decalcified in formic acid, mounted in paraffin, and sectioned on a microtome at the Musculoskeletal Research Histology Core at Washington University in St. Louis (WUSTL). Following deparaffinization, longitudinal bone sections ( $n = 3-4$  bones/group)

were stained with hematoxylin and eosin (H&E), Masson's Trichrome, or anti-CD68 (1:50; MCA341A647; Biorad).

Images were captured at  $\times 5$ ,  $\times 10$ , and  $\times 20$  magnification using a Zeiss Axiocam microscope. Slides stained with hematoxylin and eosin (H&E) were scanned to obtain composite images of the entire muscle section using an Olympus BX614S (SLU). Fluorescently labeled slides were scanned using NanoZoomer 2.0 HT (WUSTL).

### 2.5 | microCT imaging and analysis of bone fractures

microCT was used to quantify new mineralized tissue in the callus region at Days 14 and 28 ( $n = 5-8$  bones/group). A 2.2 mm length centered around the fracture site was scanned with microCT (microCT 35; ScanCo Medical; X-ray tube potential 70 kVp, integration time 300 ms, X-ray intensity 145  $\mu\text{A}$ , isotropic voxel size 12  $\mu\text{m}$ , medium resolution scan). Manual contours were drawn around the exterior of the callus and a second set of contours were drawn to exclude the long bone. A threshold for mineralized tissue was set above 255 per milles. Data of total callus volume (TV), bone volume (BV), bone volume fraction (BV/TV) and bone mineral density (BMD) were collected. To assess fracture bridging, the scout view X-ray, lateral reconstruction, and an anterior reconstruction of each scan were blindly graded by SMG as seen in Mehta et al.<sup>24</sup>—a score of 4 was assigned for complete bridging (four cortices bridged by callus), 3 for incomplete bridging (one to three cortices bridged by callus), 2 for no bridging (presence of callus but no cortex bridging at all) and 1 for pseudoarthrosis (rounding of cortex and almost no callus formation).

### 2.6 | Gene expression

As described previously,<sup>21</sup> RNA was isolated from snap-frozen tibiae ( $n = 5$  bones/group). Before RNA isolation, the soft tissue, fibula, and articulating ends were removed. Bone marrow was removed from the tibiae isolated from cage control animals by driving an intramedullary K-pin through the tibia. Bones were wrapped in a sterile piece of aluminum foil and pulverized in a liquid nitrogen chilled vessel. Following pulverization, bone fragments were collected and incubated with Trizol LS reagent (Invitrogen) for 10 min to isolate RNA, which was subsequently purified using RNeasy mini kit (Qiagen). All primer sets have been synthesized by Sigma-Aldrich DNA oligos design tool (Table 1). Immunogenic markers were analyzed using a Rat Innate and Adaptive Immune Response RT<sup>2</sup> Profiler PCR arrays (PARN052Z; SABiosciences), as described previously.<sup>14</sup>

### 2.7 | Muscle function assessment

In vivo functional testing of the anterior crural muscles ( $n = 7-10$  muscles/group) was performed at 28 days post-injury using the

**TABLE 1** Nucleotide sequence for primers used for qRT-PCR

Gene	Forward sequence	Reverse sequence	Amplicon length (bp)
18s	5'-GGCCCGAAGCGTTTACTT-3'	5'-ACCTCTAGCGGCGCAATAC-3'	173
CCR7	5'-GCTCTCCTGGTCATTTTCCA-3'	5'-AAGCACACCGACTCATACAGG-3'	107
CD163	5'-TCATTTGGAAGAAGCCCAAG-3'	5'-CTCCGTGTTTCACTTCCACA-3'	101
TNF- $\alpha$	5'-ACTCGAGTGACAAGCCCGTA-3'	5'-CCTTGTCCTTGAAGAGAACC-3'	184
TNF- $\beta$ 1	5'-GTCAGACATTCGGAAGCA-3'	5'-CCAAGGTAACGCCAGGAAT-3'	138

methodology previously described.<sup>25</sup> Briefly, peak physiological properties were analyzed from anesthetized rats (isoflurane 1.5%–2.0%) using a dual-mode muscle lever system (Aurora Scientific, Inc., Mod. 305b). The Achilles tendon was severed to avoid stimulated plantarflexion of the foot. The ankle was mounted in the foot pedal and secured at a right angle. Subcutaneous platinum electrodes were placed on each side of the peroneal nerve. Optimal current (30–40 mA) was set through a series of increasing twitches. Isometric tetanic contractions were elicited through stimulation at 150 Hz (0.1 ms pulse width, 400 ms train).

## 2.8 | Statistical analysis

Data are presented as a mean  $\pm$  standard error. Analysis and graphing of data were performed using GraphPad Prism 8 for Windows. Because only the animals sacrificed at the Day 28 time-point received enrofloxacin treatment, the data from these animals is presented separately from the Day 7 and 14 time-points. Sample-sizes were selected based on power analysis on pilot data. A one-way or two-way analysis of variance (ANOVA) was used when appropriate to determine if there was a significant interaction or main effect between variables. The Fisher's least significant difference post hoc comparison was performed to identify significance with  $p < .05$ . The PCR immunoarray data analysis was carried out with the online RT<sup>2</sup> Profiler PCR Array Data Analysis version 3.5 to determine fold regulation of genes.

## 3 | RESULTS

### 3.1 | Muscle mass and function

The TA muscle mass was normalized to the body weight of the animal. VML+OST injured animals had a significantly lower normalized TA mass than the control at Days 7 and 14 (two-way ANOVA interaction  $p = .0215$ , time factor  $p = .0098$ , treatment factor  $p < .0001$ ) (Figure 1A). On Day 28 after the VML+OST injury, a deficit of ~37% and ~29% was observed between the untreated and treated muscles compared to control (one-way ANOVA  $p < .001$ ) (Figure 1B).

Peak isometric torque was measured on 28 days post-injury (Figure 1C). The OST injury alone creates a functional deficit of ~16%–17% compared to controls (Table 2) potentially suggesting disuse atrophy in the TA muscles. As expected, the injured muscles in the VML+OST group produced significantly lower torque compared to both control and OST-only muscles (Figure 1C).

When normalized to animal body weight, no statistical differences were noted between the control and OST groups. But the VML+OST muscles produced significantly lower torque compared to the control muscles (one-way ANOVA  $p < .0001$ ) (Figure 1D and Table 2). Sponge treated VML+OST muscles showed a statistically higher peak torque (~52%) compared to untreated muscles.

When normalized to the TA muscle mass, the OST groups were statistically similar but the VML+OST muscles were statistically lower compared to the controls. (one-way ANOVA  $p < .0001$ ). No differences were observed between treated and untreated muscles (Figure 1E).

### 3.2 | Cellular infiltration, myofiber regeneration, fibrosis

The inflammatory cell infiltration was similar in both treated and untreated muscles. Qualitative analysis revealed T cells (CD3<sup>+</sup>) around the periphery but macrophages (CD68<sup>+</sup>) infiltrating the implanted sponges at Day 7 (Figure 2). Both groups supported endothelial (CD31<sup>+</sup>) and stem cell (SCA1<sup>+</sup>) activity in the muscle defect suggesting that the biomimetic sponges are not detrimental to angiogenesis or stem cell infiltration. Muscle fibers with acetylcholine receptor clustering ( $\alpha$ -bungarotoxin<sup>+</sup>) indicating post-synaptic terminals were similar in both untreated and treated muscles at Day 28 (Figure S1A).

Sponge-treated muscles showed several small myofibers (MHC<sup>+</sup>) growing throughout the defect (Figure 3). The ratio of MHC:COL (% area) provided quantitative analysis of muscle regeneration and fibrosis (Figure 3D). At Day 28, sponge-treated muscles had a significantly higher MHC:COL ratio compared to untreated muscles (one-way ANOVA  $p < .0001$ ). MHC:COL ratios of both VML+OST injured groups were significantly lower than control. No differences in MHC:COL ratio were seen between untreated and treated VML+OST groups at Day 7 or 14 (Figure S1B).

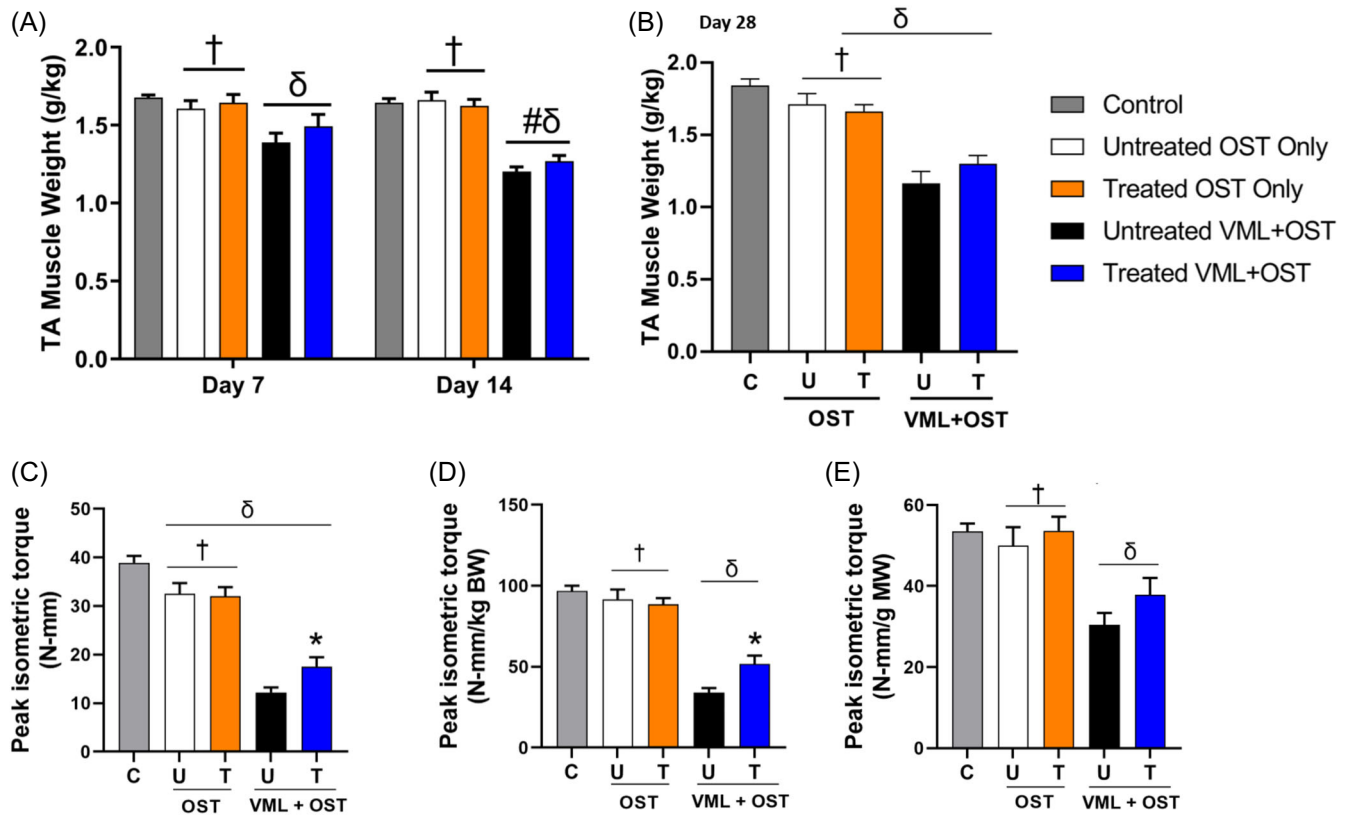


**FIGURE 1** Composite volumetric muscle loss and osteotomy (VML+OST) injury has a detrimental effect on (A,B) TA muscle mass over 28 days post-injury regardless of treatment. VML+OST injury decreases (C) peak isometric torque (raw values), (D) peak torque normalized to body weight (BW) of the animal, as well as (E) peak torque normalized to TA muscle weight (MW). (C,D) Biomimetic sponge implantation significantly enhances peak torque in the composite injury animals. (δ) indicates statistical significance ( $p < .05$ ) compared to control. (\*) indicates statistical significance ( $p < .05$ ) compared to corresponding treatment group. (†) indicates statistical significance ( $p < .05$ ) between injury groups. (#) indicates statistical significance ( $p < .05$ ) over Day 7 time point [Color figure can be viewed at [wileyonlinelibrary.com](http://wileyonlinelibrary.com)]

### 3.3 | Muscle CSA

Myofiber CSA and count were calculated from whole sections at Days 14 and 28 (Figure 4A,B). On Day 28, the sponge-treated muscle had significantly higher mean myofiber CSA than untreated muscle (one-way ANOVA  $p = .0114$ ) (Figure 4C). Additionally, mean myofiber CSA was significantly lower in the untreated group compared to the control at Day 28, potentially suggesting ongoing degeneration in the untreated muscles.

Total myofiber number was significantly higher with sponge treatment compared to untreated at Days 14 and 28 (one-way ANOVA  $p < .0001$ ) (Figure 4D,E). VML injury resulted in a ~76% and ~48% deficit in myofiber number on Day 14 in untreated and treated muscles, respectively.

Fiber-size distribution analysis revealed a significantly higher number of small diameter myofibers ( $< 500 \mu\text{m}^2$ ) and larger fibers ( $500\text{--}999$ ,  $1000\text{--}1499$ , and  $1500\text{--}1999 \mu\text{m}^2$ ) were present in sponge treated muscle compared to untreated muscle at Day 14 (two-way ANOVA Interaction  $p < .0001$ , time factor  $p < .0001$ , treatment factor  $p < .0001$ ) (Figure 5A). By Day 28, a significantly higher quantity of fibers between 500 and 999, and 1000–1499  $\mu\text{m}^2$  were seen in sponge treated groups

fibers between 1500 and 1999  $\mu\text{m}^2$  trended higher ( $p = .0530$ ) over untreated (two-way ANOVA Interaction  $p < .0001$ , time factor  $p < .0001$ , treatment factor  $p < .0001$ ) (Figure 5B).

### 3.4 | Innate and adaptive immune response

The circulating serum levels of IL-2 were found significantly lower in the sponge-treated VML+OST group compared to the untreated VML+OST group on Day 7 (two-way ANOVA Interaction  $p = .2238$ , Injury Factor  $p = .0945$ , Treatment factor  $p = .0431$ ). No differences were observed on Day 14 post-injury (Figure 6A).

Gene expression of treated VML+OST muscle samples was directly compared to untreated samples. At Day 7 post-injury, sponge treatment appears to have immunomodulatory effects at the site of injury (Figure 6B). Of the 84 genes analyzed, none were upregulated in the sponge group compared to untreated, but 44 genes were downregulated. Of these 44 genes, CD4, CD8a, CXCR3, IFNGR1, IRAK1, and CSF2 were significantly downregulated in sponge treated muscle compared to unrepaired samples ( $p < .05$ ).

**TABLE 2** Morphological characteristics and deficits. Symbols indicate statistical significance ( $p < 0.05$ ) compared to control ( $\delta$ ), corresponding treatment group (\*), between injury groups ( $\dagger$ ), and day 7 time point ( $\#$ ) and day 14 ( $\phi$ ).

	Control			Untreated OST Only			Treated OST Only			Untreated VML+OST			Treated VML+OST		
	Day 7	Day 14	Day 28	Day 7	Day 14	Day 28	Day 7	Day 14	Day 28	Day 7	Day 14	Day 28	Day 7	Day 14	Day 28
Body Weight (kg)	0.320	0.369#	0.377#	0.285 $\delta$	0.333# $\delta$	0.361#	0.315* $\delta$	0.339 $\delta$	0.353#	0.291 $\delta$	0.325# $\delta$	0.358	0.291 $\delta$	0.323# $\delta$	0.362
Normalized TA Mass (g/kg)	1.677	1.644	1.842# $\phi$	1.607 $\dagger$	1.661 $\dagger$	1.712 $\dagger$	1.644 $\dagger$	1.624 $\dagger$	1.663 $\dagger\delta$	1.389 $\delta$	1.202 $\delta$ #	1.165 $\delta$	1.492 $\delta$	1.270 $\delta$ #	1.301 $\delta$
% Deficit to Control	-	-	-	4.194 $\dagger$	-1.00 $\dagger$	-7.02 $\dagger$	1.983	1.251 $\dagger$	9.714	17.173	26.888#	36.734	11.00	22.78#	29.34
% Recovery to Untreated	-	-	-	-	-	-	2.307	-2.230	-2.897 $\dagger$	-	-	-	7.45	5.63	11.69
Normalized EDL Mass (g/kg)	0.378	0.377	0.407	0.372	0.427	0.421	0.409	0.409	0.413	0.417	0.440 $\delta$	0.456	0.451 $\delta$	0.435	0.461
Peak Isometric Torque (N-mm)	-	-	38.91	-	-	32.51 $\dagger\delta$	-	-	32.01 $\dagger\delta$	-	-	12.18 $\delta$	-	-	17.53* $\delta$
% Function Deficit to Control	-	-	-	-	-	16.44 $\dagger$	-	-	17.73 $\dagger$	-	-	68.70	-	-	54.94*
% Function Recovery to Untreated	-	-	-	-	-	-	-	-	-1.538	-	-	-	-	-	43.96
Peak Isometric Torque Normalized to BW (N-mm/kg)	-	-	96.87	-	-	91.39 $\dagger$	-	-	88.50 $\dagger$	-	-	33.96 $\delta$	-	-	51.64* $\delta$
% Function Deficit to Control	-	-	-	-	-	5.658 $\dagger$	-	-	8.640 $\dagger$	-	-	64.94	-	-	46.70*
% Function Recovery to Untreated	-	-	-	-	-	-	-	-	-3.161	-	-	-	-	-	52.04
Peak Isometric Torque Normalized to TA Mass (N-mm/g)	-	-	53.46	-	-	49.97 $\dagger$	-	-	53.63 $\dagger$	-	-	30.49 $\delta$	-	-	37.82 $\delta$
% Function Deficit to Control	-	-	-	-	-	6.521 $\dagger$	-	-	-3.209 $\dagger$	-	-	42.96	-	-	29.24
% Function Recovery to Untreated	-	-	-	-	-	-	-	-	7.319	-	-	-	-	-	24.05



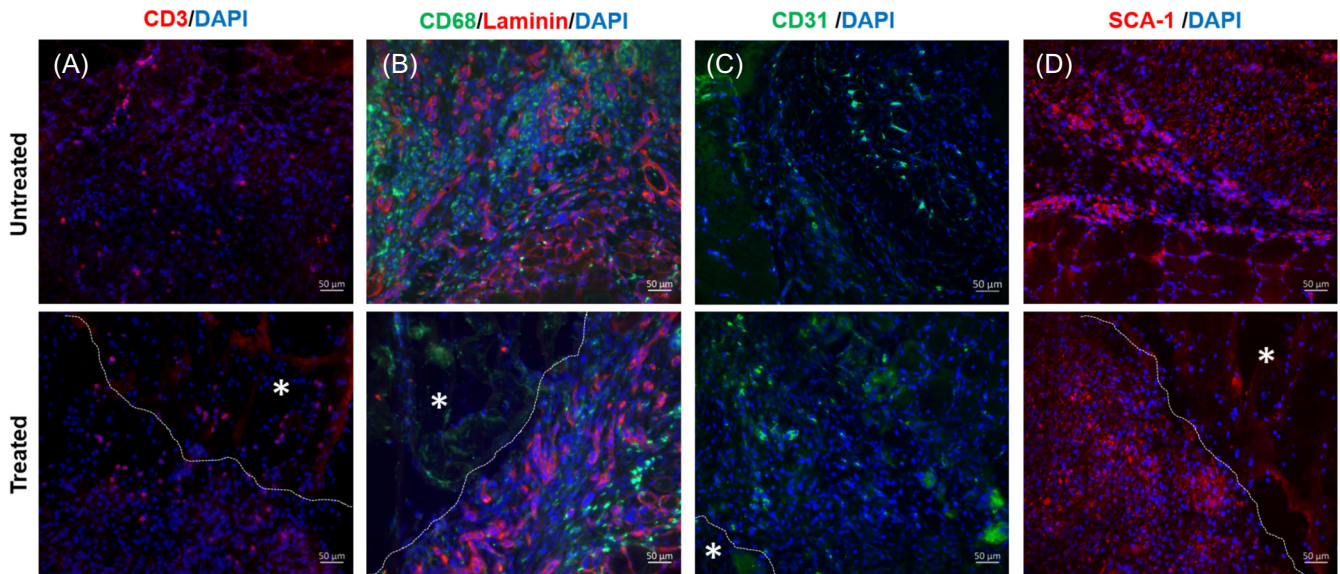


**FIGURE 2** Immunohistological staining shows (A,B) T cells (CD3<sup>+</sup>) and macrophages (CD68<sup>+</sup>) infiltrating the defect area on Day 7 post-injury. CD3<sup>+</sup>T cells surround the sponge (\*) whereas CD68<sup>+</sup> macrophages are shown infiltrating the remodeled sponge. (C,D) Endothelial cells (CD31<sup>+</sup>) and stem cells (SCA-1<sup>+</sup>) migrate throughout the entire defect. Scale bar = 50 μm. The white dashed line indicates the approximate boundary between the implanted sponge and the surrounding musculature [Color figure can be viewed at [wileyonlinelibrary.com](http://wileyonlinelibrary.com)]

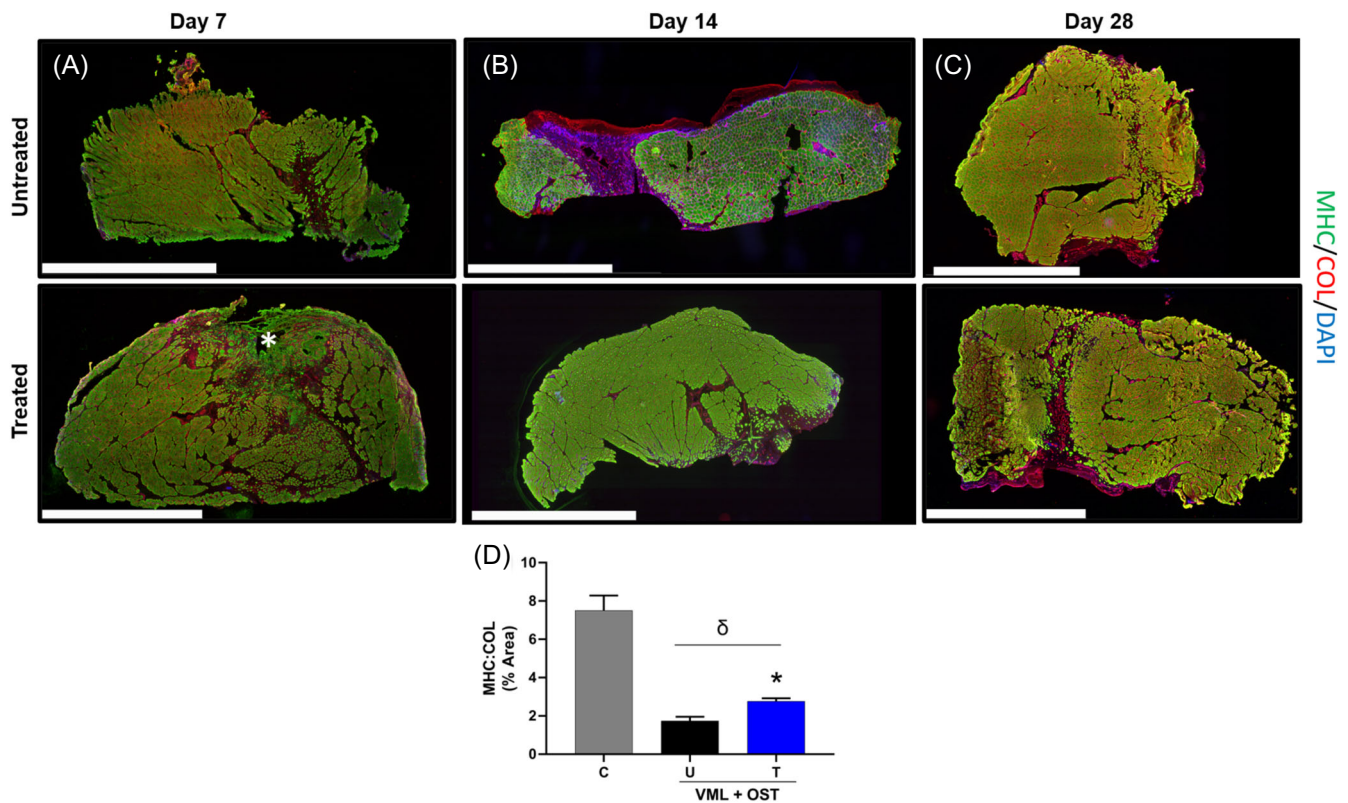


**FIGURE 3** Muscle cross-sections were stained with myosin heavy chain (MHC) and collagen (COL). (A-C) Sponge treatment provides support and retention of healthy architecture. The sponge (\*) is still visible at Day 7. (D) Muscle Regeneration and fibrosis were quantified by MHC:COL ratio. On Day 28, sponge treatment significantly improves MHC:COL ratio over untreated muscle. Scale Bars are each 3 mm. (\*) indicates statistical significance ( $p < .05$ ) between treatment groups at each time point. (δ) indicates a statistical difference compared to control [Color figure can be viewed at [wileyonlinelibrary.com](http://wileyonlinelibrary.com)]

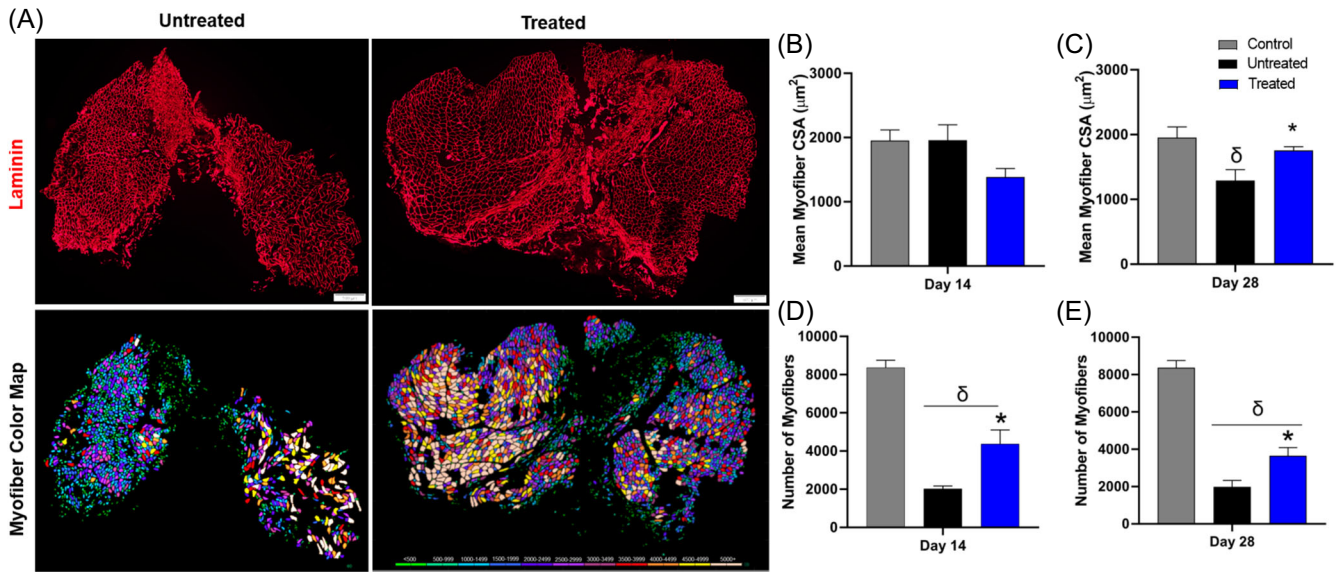


**FIGURE 4** Laminin-stained muscle sections were analyzed to calculate myofiber cross-sectional area (CSA). (A) Immunostained images and color-coded maps of Day 28 samples are displayed. Mean myofiber CSA on (B) Day 14 and (C) Day 28 are shown. The total number of myofibers increase with sponge treatment on both (D) Day 14 and (E) Day 28. ( $\delta$ ) indicates statistical significance ( $p < .05$ ) compared to control. (\*) indicates statistical significance ( $p < .05$ ) compared to the corresponding treatment group. Cage control group is the same for Days 14 and 28 [Color figure can be viewed at [wileyonlinelibrary.com](http://wileyonlinelibrary.com)]

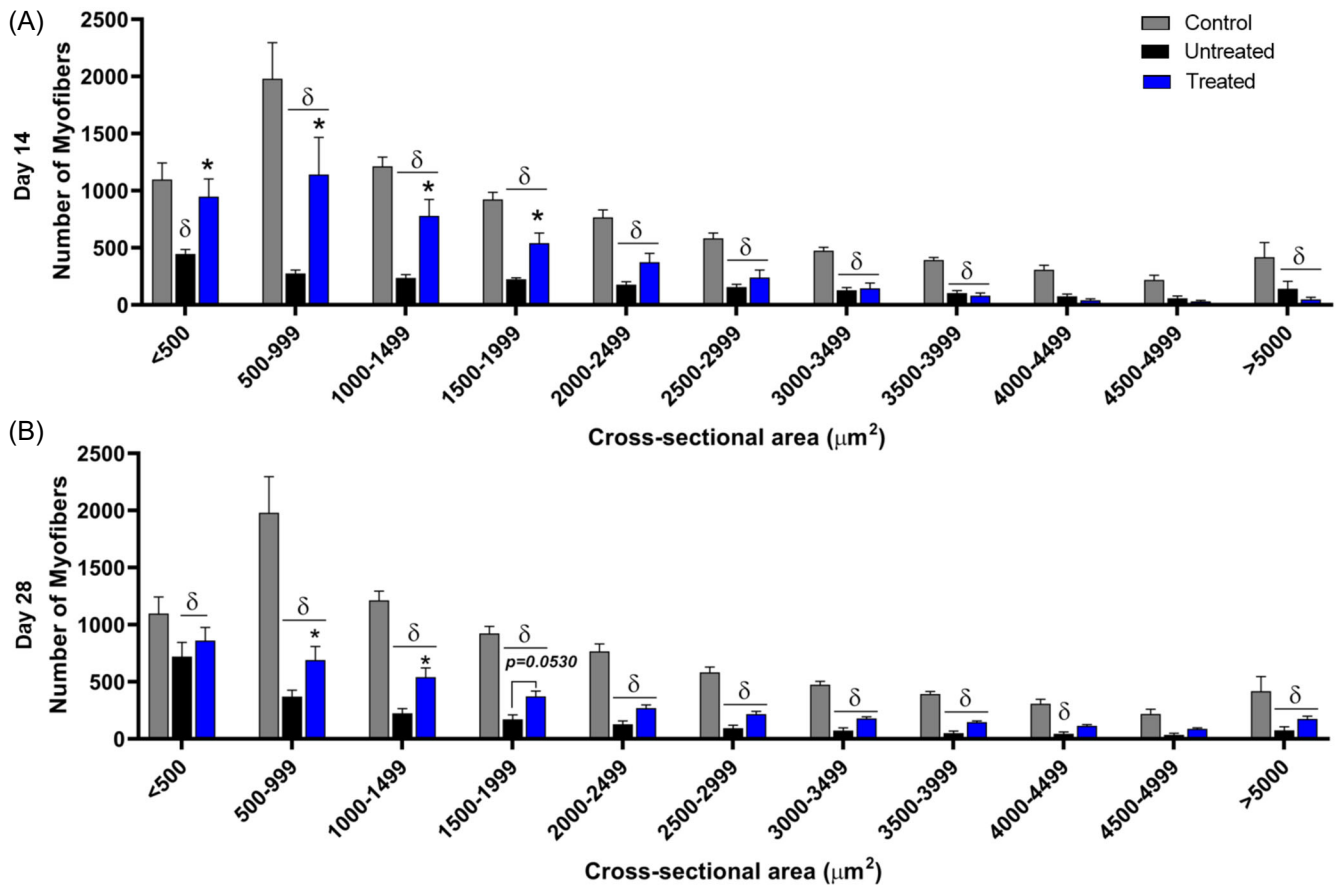


**FIGURE 5** Myofiber size distribution is shown. Sponge treatment improves quantity of larger mature fibers at Days 14 (A) and 28 (B) post-injury. ( $\delta$ ) indicates statistical significance ( $p < .05$ ) compared to control. (\*) indicates statistical significance ( $p < .05$ ) compared to corresponding treatment group. Cage control group is the same for Days 14 and 28 [Color figure can be viewed at [wileyonlinelibrary.com](http://wileyonlinelibrary.com)]



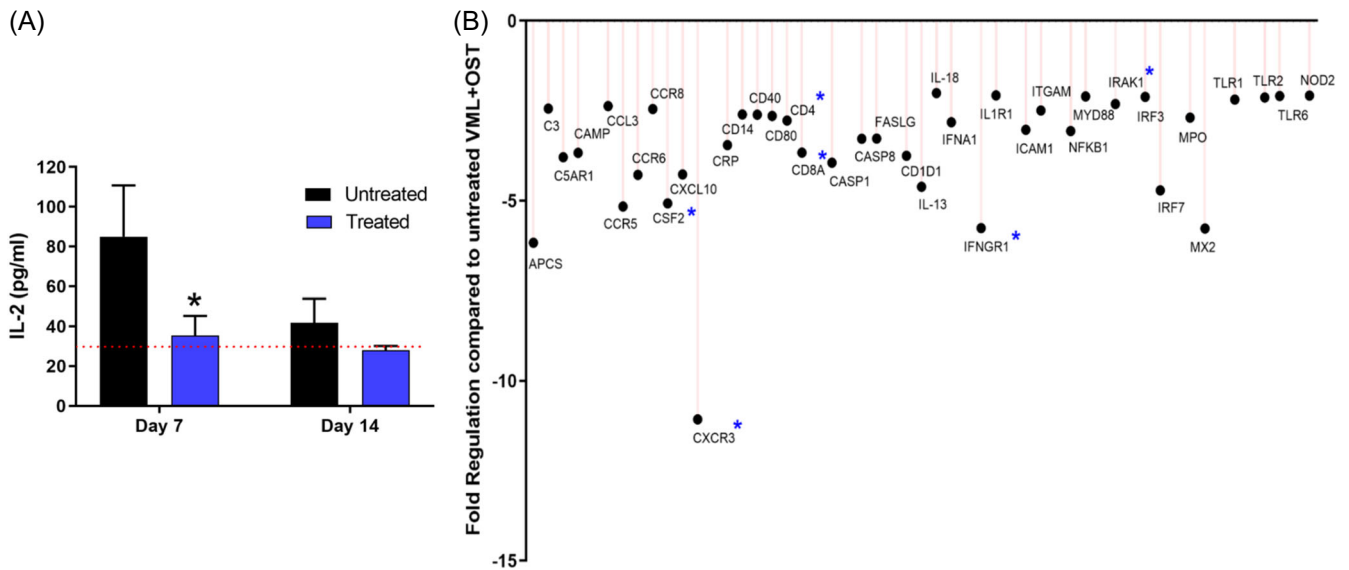


**FIGURE 6** (A) The circulating serum levels of interleukin-2 (IL-2) were quantified by enzyme-linked immunosorbent assay (ELISA) in the composite trauma (volumetric muscle loss [VML]+osteotomy [OST]) group. Sponge treatment significantly reduced circulating levels of interleukin-2 (IL-2) on Day 7 post-injury. The broken red line indicates the average IL-2 concentration in the cage control animals. (B) An array of immunogenic markers was quantified via polymerase chain reaction (PCR). Biomimetic sponge implantation in VML+OST injured muscle downregulated 44 genes. Of those downregulated genes, CSF2, CXCR3, CD4, CD8a, IFNGR1 and IRAK1 were significantly downregulated with sponge treatment. (\*) indicates a significant difference ( $p < .05$ ) compared to untreated expression [Color figure can be viewed at [wileyonlinelibrary.com](http://wileyonlinelibrary.com)]

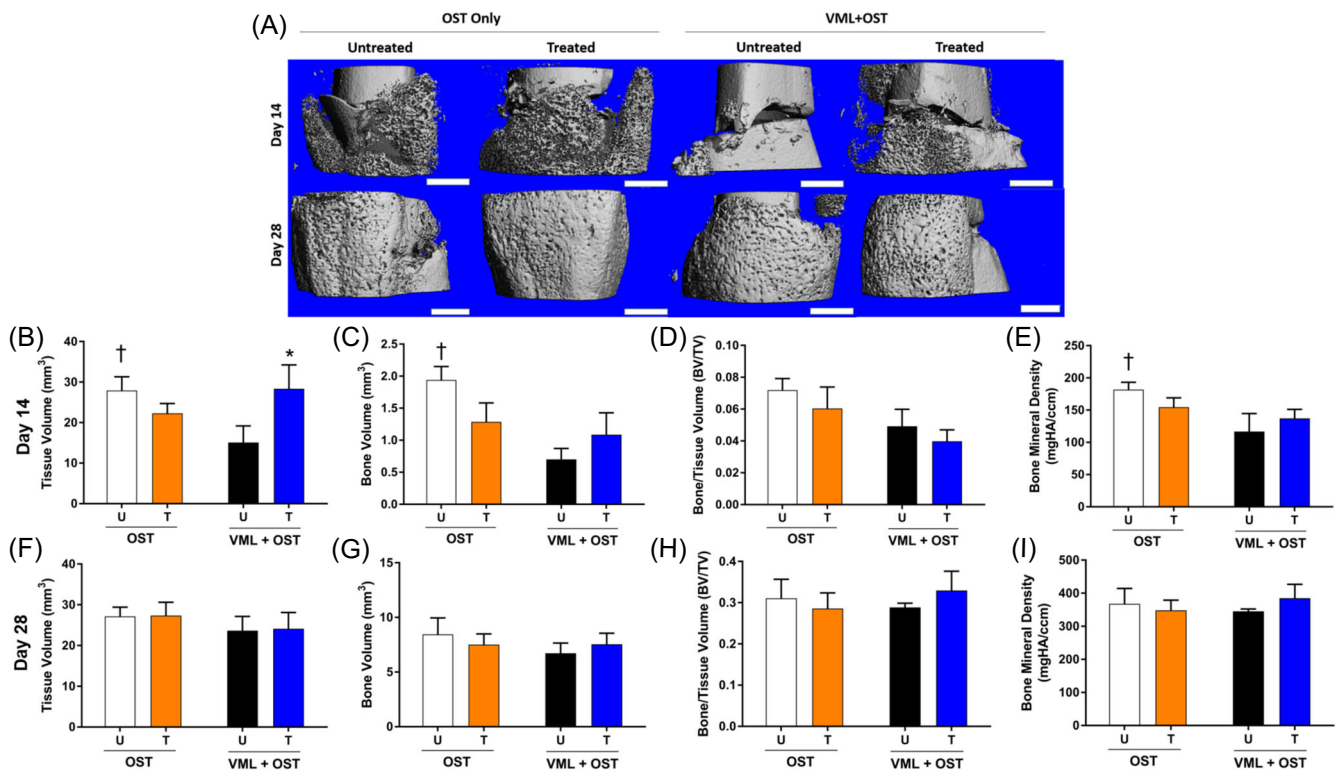


**FIGURE 7** MicroCT analysis was performed to quantify fracture healing. (A) Representative 3D reconstructions of fracture calluses at Days 14 and 28. Volumetric muscle loss (VML)+osteotomy (OST) injury significantly decreased (B) callus or tissue volume (TV), (C) mineralized bone volume (BV) and (E) bone mineral density (BMD) on Day 14. No differences were seen in (D) bone volume fraction (BV/TV). Compared to untreated VML+OST muscles, sponge treatment increased TV on Day 14. The symbol (†) indicates a significant difference ( $p < .05$ ) between injury groups and (\*) indicates difference between treatment groups. Scale bar = 1 mm [Color figure can be viewed at [wileyonlinelibrary.com](http://wileyonlinelibrary.com)]

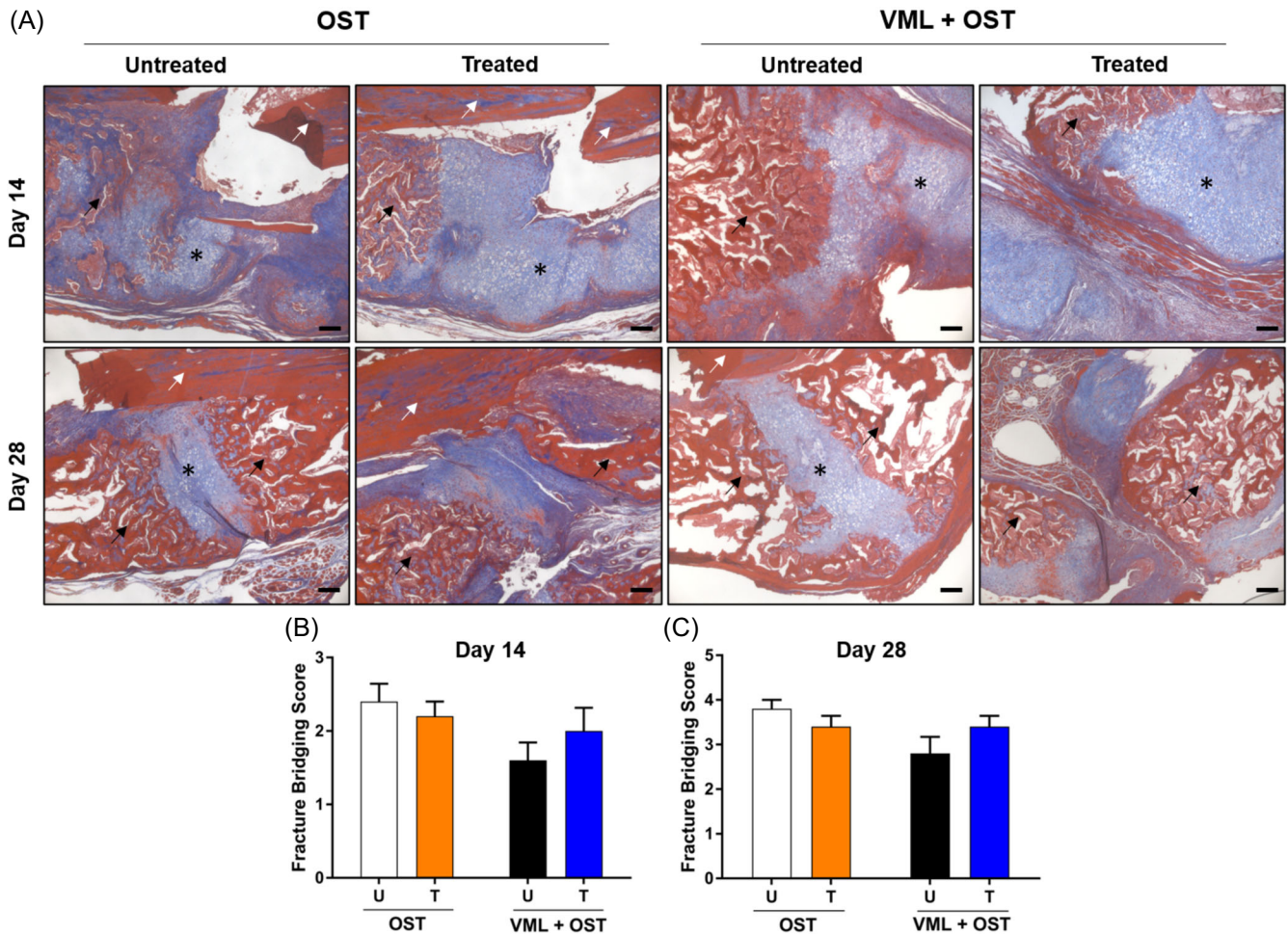


**FIGURE 8** (A) Masson's Trichrome stains of fracture sites at Days 14 and 28. As healing occurs between Days 14 and 28, the cartilaginous callus consisting of hypertrophic chondrocytes (\*) becomes more mineralized (black arrows) regardless of trauma intensity. White arrows indicate long bone in the fracture callus. All images are at  $\times 5$  magnification. Scale bar = 200  $\mu\text{m}$ . (B,C) MicroCT reconstructions were evaluated for cortex bridging along each axis on Days 14 and 28, with a score of 4 indicating complete bridging and 1 indicating pseudoarthrosis [Color figure can be viewed at [wileyonlinelibrary.com](http://wileyonlinelibrary.com)]

### 3.5 | Fracture callus characterization

Ex vivo microCT was performed on fractured tibia calluses from OST and VML+OST injured animals on Days 14 and 28 post-injury (Figure 7A). VML+OST injury significantly decreased tissue volume (TV) at Day 14 (two-way ANOVA Interaction  $p = .0369$ , Injury Factor  $p = .4268$ , Treatment factor  $p = .3411$ ) (Figure 7B). Sponge treatment significantly increased TV over untreated VML+OST. Mineralized bone volume (BV) was decreased in the VML+OST group at Day 14 compared to OST alone (two-way ANOVA Interaction  $p = .0661$ , Injury factor  $p = .0147$ , Treatment factor  $p = .6165$ ) (Figure 7C). The BV/TV ratio showed a significant injury effect ( $p = .0460$ ) at Day 14 (Figure 7D). The bone mineral density (BMD) decreased in untreated VML+OST injured animals at Day 14 compared to OST only (two-way ANOVA interaction  $p = .2075$ , Injury factor  $p = .0369$ , Treatment factor  $p = .8488$ ) (Figure 7E). By Day 28, all groups had statistically similar levels of TV, BV, and BMD.

Masson's Trichrome staining (Figure 8A) showed that the callus appeared much more cartilaginous as indicated by the blue-staining fibrous tissue than mineralized as indicated by red-staining new bone in all groups at Day 14. By Day 28, more mineralization had occurred, leaving smaller areas of hypertrophic chondrocytes at the defect site. Fracture bridging scores showed a trend towards injury effect at Day 14 ( $p = .0675$ ). On Day 28, fracture bridging scores showed a trending interaction ( $p = .0866$ ) and injury effect ( $p = .0866$ ), indicating that an adjacent VML injury has an overall negative impact tibia healing (Figure 8B,C).

Macrophages (CD68<sup>+</sup>) cells can be seen in the mineralized callus of fractures at Day 14 (Figure 9). On Day 7 post-injury, the gene expression of CCR7 (two-way ANOVA interaction  $p = .9034$ , Injury factor  $p = .8290$ , Treatment factor  $p = .0533$ ) and TGF- $\beta$ 1 (two-way ANOVA Interaction  $p = .6894$ , Injury factor  $p = .1966$ , Treatment factor  $p = .0895$ ) trended towards an increase in the sponge treated OST and VML+OST groups. A significant treatment effect was

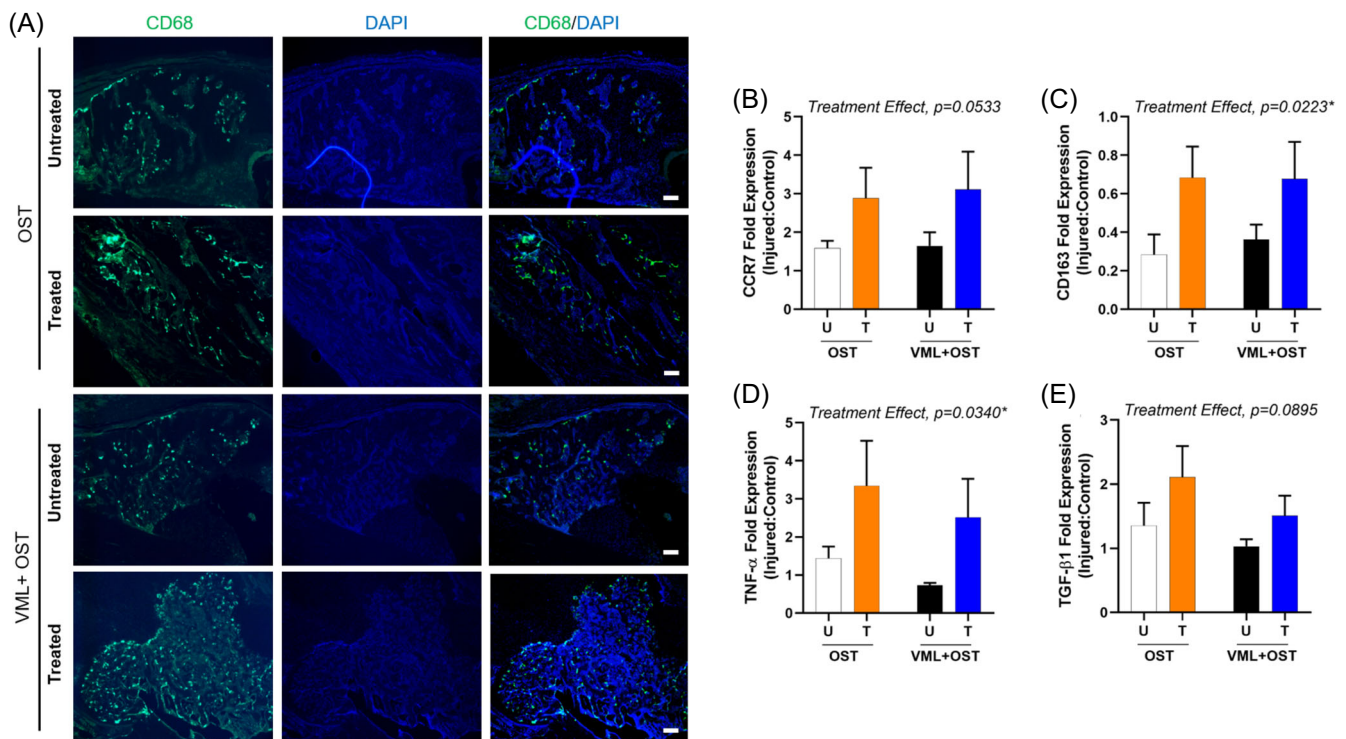


**FIGURE 9** (A) Macrophages (CD68<sup>+</sup>) in fracture calluses at Day 14 post-injury. Inflammatory cells in the fracture site are visible in both injury groups. These cells are located around mineralized tissue. All images are at  $\times 5$ . Scale bar=200  $\mu$ m. Gene expression of (B) CCR7, (C) CD163, (D) TNF- $\alpha$ , and (E) TGF- $\beta$ 1 was quantified by qPCR on Day 7 post-injury [Color figure can be viewed at [wileyonlinelibrary.com](http://wileyonlinelibrary.com)]

observed in the gene expression of CD163 (two-way ANOVA Interaction  $p = .7668$ , Injury factor  $p = .8008$ , Treatment factor  $p = .0223$ ) and TNF- $\alpha$  (two-way ANOVA Interaction  $p = .9440$ , Injury factor 0.3482, Treatment factor  $p = .0340$ ) suggesting higher expression in the sponge treated OST and VML+OST groups. While the CD68<sup>+</sup> macrophages persisted in the defect for 14 days, the gene expression of CCR7 and CD163 was not statistically different between the groups on Day 14 post-injury (Figure S2).

## 4 | DISCUSSION

Despite ample preclinical and clinical evidence on the crucial role of intact muscle tissue in augmenting bone fracture healing, a targeted therapy for VML injury currently does not exist. We developed an immunomodulatory and regenerative therapy to address this gap in orthopedic care. Our results show that in a model of composite muscle-bone trauma, FK-506 loaded biomimetic sponges modulated the pro-inflammatory immune response, and increased peak torque, MHC:COL ratio, mean myofiber CSA, as well as the total number of myofibers in the VML injured muscles.

Previous studies involving composite trauma have focused primarily on bone healing. For instance, Willett et al.,<sup>26</sup> showed that femur fractures treated with recombinant human bone morphogenetic protein (rhBMP)-2 loaded alginate gels showed severely impaired healing when challenged with an adjacent untreated VML

injury in the quadriceps. In subsequent studies, BMP-2 was delivered via collagen hydrogels,<sup>27</sup> or sponges,<sup>28</sup> for bone healing. However, treatments for VML injury were not developed or investigated.

We are only aware of one other published study where different tissue engineering strategies were used to repair both injured muscle and bone fracture in a composite trauma model.<sup>29</sup> Pollot et al., repaired VML injured TA muscle with a SIS-ECM scaffold and the adjacent tibia fracture with rhBMP-2 loaded collagen sponge. SIS-ECM implantation in the VML defect did not improve muscle strength and impaired adjacent BMP-2 mediated bone fracture healing.<sup>29</sup> The authors suggested that SIS-ECM implantation exacerbated the chronic inflammation observed at the VML site of injury which resulted in poor healing outcomes in both muscle and bone tissues.

In this study, we hypothesized that biomimetic sponges containing FK-506 and ECM proteins (e.g., gelatin, collagen, and LM-111) provide both regenerative and anti-inflammatory effects to the injured tissues. To characterize the acute inflammatory response following biomimetic sponge implantation, gene expression of innate and adaptive immune mediators was investigated. Injured muscles typically show increased expression of chemokines,<sup>30,31</sup> which control immune cell recruitment and inflammation by binding specific receptors on target cells. The gene expression of colony-stimulating factor-2 (CSF-2) (also known as GM-CSF) and CXCR3 was significantly downregulated -5.07-fold and -11.07-fold, respectively. Skeletal muscle-derived CSF-2 is known to promote neutrophil chemotaxis after strain-induced injury.<sup>32</sup> T cells express the receptor



CXCR3, which binds to the chemokine CXCL10, and this interaction is important for peripheral homing of T cells. The binding of CXCL10 to CXCR3 can also initiate inflammation, promote apoptosis, and reduce angiogenesis.<sup>33–36</sup> The average expression of CXCL10 was downregulated –4.27-fold, but statistical significance was not achieved. Taken together, these results suggest that a reduction in key growth factor and/or chemokine signaling, and activity might limit the infiltration of immune cells into our biomimetic sponges. IL-2 is required for T cell autocrine signaling and a reduction in circulating IL-2 levels might indicate reduced T cell activity and proliferation. A significant downregulation in the gene expression of CD4 (–2.77-fold) and CD8a (–3.66-fold) in sponge treated muscles further supports limited T cell activity on Day 7 post-injury.

IRAK1 plays an essential role in nuclear factor (NF- $\kappa$ B) activation. Several transcripts involved in the NF- $\kappa$ B pathway were downregulated with sponge treatment. NF- $\kappa$ B has been implicated in muscle wasting and atrophy,<sup>37–39</sup> and its reduced activity might preserve muscle mass following VML injury. IFN- $\gamma$ R1 is expressed on several immune cells and myofibers.<sup>40</sup> Downregulation of IFN- $\gamma$ R1, on immune cells and myofibers is likely to make them less responsive to the effect of pro-inflammatory cytokines. One study reported ligand-independent downregulation of IFN- $\gamma$ R1 on activated T cells with cyclosporine A,<sup>41</sup> a drug with similar mechanism of action to FK-506. It is possible that the downregulation of this receptors on immune cells and myofibers in sponge treated muscles is offering protection against the damaging effect of pro-inflammatory cytokines in the VML microenvironment. However, more studies are needed to substantiate this claim.

A significant increase in the number of small myofibers (<500  $\mu\text{m}^2$ ), potentially suggesting regenerating myofibers, was observed in the sponge treated group. Compared to untreated muscles, larger myofibers (500–2000  $\mu\text{m}^2$ ), indicative of ongoing maturation, were also increased in the sponge treated group on both Days 14 and 28 postimplantation. Sponge treatment also increased the total number of myofibers as well as the mean myofiber CSA compared to untreated muscles on Day 28. An overall increase in myosin<sup>+</sup> myofibers was further confirmed by the higher MHC:COL ratio in the sponge treated muscles on Day 28. These results suggest that the observed increase in peak torque production is due to increased contractile tissue in sponge treated muscles and cannot be attributed to functional fibrosis, previously observed with decellularized ECM scaffolds.<sup>21</sup>

To assess fracture healing,  $\mu$ CT quantification of bone formation was performed on Days 14 and 28 post-injury. On Day 14, the TV, BV, and BMD were significantly lower in the composite injury group compared to OST only groups, indicating that fracture healing is impaired with an adjacent VML.<sup>14,25,26</sup> However, all fractures were found bridged at Day 28, as expected with this endogenously healing bone fracture model. It is possible that increased immune cell migration from VML injured muscle to fractured bone might have affected adjacent bone healing. The detrimental role of inflammation in fracture repair is highlighted by studies which show that genetic ablation of adaptive immune cells supports bone healing,<sup>42</sup> while increased presence of cytotoxic T cells can delay recovery.<sup>43</sup>

Sponge treatment significantly increased the TV at Day 14 (suggesting a larger callus) but did not improve mineralized bone content. Gene expression data on Day 7 suggests increased presence of anti-inflammatory macrophages (CD163<sup>+</sup>) as well as pro-inflammatory cytokines (TNF- $\alpha$ ) in the sponge treated bones. Therefore, unlike muscle tissue, immunosuppression was not observed in fractured tibias.

This study had some limitations. For instance, previous studies using a similar composite trauma model utilized a larger threaded pin (1.25 mm) to stabilize both ends of the fracture.<sup>6,14</sup> While the use of thinner pin (0.7 mm) for fractured tibia fixation has been previously published,<sup>44,45</sup> it may have provided less than ideal stability to the fracture site. Another limitation associated with this study is the lack of a control group consisting of biomimetic sponges without FK-506. Future studies will investigate the extent of regeneration and immunomodulation observed with biomimetic sponges in the absence of a locally delivered immunomodulatory drug. The extent to which physical rehabilitation can improve functional recovery following sponge implantation will be investigated in future studies.

## ACKNOWLEDGMENTS

This study was supported by a grant from the National Institute of Health (NIGMS) 1R15GM129731 awarded to Koyal Garg. We would like to thank Gary D. London (Washington University), as well as Caroline Murphy and Dr. Grant Kolar (Saint Louis University) for technical assistance with histological imaging and Frank Strebeck (Saint Louis University) for help with radiographic imaging.

## CONFLICT OF INTERESTS

GenAssist, Inc. is developing products related to the research described in this paper. Koyal Garg has equity interest in GenAssist, Inc., and serves on the company's scientific advisory board. The terms of this arrangement have been reviewed and approved by Saint Louis University, in accordance with its conflict-of-interest policies. Gabriel Haas is the CEO and Joshua Madsen is the CTO of GenAssist, Inc. and both are members of the board of directors. AJD also holds equity interest in GenAssist, Inc.

## AUTHOR CONTRIBUTIONS

Koyal Garg and Sara McBride Gagyi designed the study. Andrew Dunn and Gabriel Haas performed the experiments. Andrew Dunn, Gabriel Haas, and Joshua Madsen collected data and performed data analysis. Andrew Dunn, Gabriel Haas, and Koyal Garg made the figures and wrote the manuscript. Natalia Ziemkiewicz, Jeffrey Au, David Johnson, Charles West, Hannah Chauvin assisted with data collection and analysis.

## ORCID

Sara McBride Gagyi  <https://orcid.org/0000-0003-2652-7997>

Koyal Garg  <http://orcid.org/0000-0002-8353-0212>

## REFERENCES

1. By the Numbers - MSK Injuries.pdf. The Burden of Musculoskeletal Diseases in the United States 2018 7/8/2020]; Available from:



- <https://boneandjointburden.org/docs/By%20The%20Numbers%20-%20MSK%20Injuries.pdf>
2. Nakamura, Y., Miyaki S., Ishitobi H., et al. Mesenchymal-stem-cell-derived exosomes accelerate skeletal muscle regeneration. *FEBS Lett.* 2015;589(11):1257-1265.
  3. Cross WW, 3rd, Swiontkowski MF. Treatment principles in the management of open fractures. *Indian J Orthop.* 2008;42(4):377-386.
  4. Garg, K., C.L. Ward, B.J. Hurtgen, et al. Volumetric muscle loss: persistent functional deficits beyond frank loss of tissue. *J Orthop Res.* 2015;33(1):40-46.
  5. Hurtgen BJ, Ward CL, Wager Leopold CM, et al. Autologous minced muscle grafts improve endogenous fracture healing and muscle strength after musculoskeletal trauma. *Physiol Rep.* 2017;5(14).
  6. Hurtgen BJ, Henderson BEP, Ward CL, et al. Impairment of early fracture healing by skeletal muscle trauma is restored by FK506. *BMC Musculoskelet Disord.* 2017;18(1):253.
  7. Roberts TT, Rosenbaum AJ. Bone grafts, bone substitutes and orthobiologics: the bridge between basic science and clinical advancements in fracture healing. *Organogenesis.* 2012;8(4):114-124.
  8. Schlickewei CW, Kleinertz H, Thiesen DM, et al. Current and Future Concepts for the Treatment of Impaired Fracture Healing. *Int J Mol Sci.* 2019;20(22).
  9. Aurora A, Garg K, Corona BT, Walters TJ. Physical rehabilitation improves muscle function following volumetric muscle loss injury. *BMC Sports Sci Med Rehabil.* 2015;6(1):41.
  10. Ward CL, Ji L, Corona BT. An Autologous Muscle Tissue Expansion Approach for the Treatment of Volumetric Muscle Loss. *Biores Open Access.* 2015;4(1):198-208.
  11. Li MT, Willett NJ, Uhrig BA, Guldberg RE, Warren GL. Functional analysis of limb recovery following autograft treatment of volumetric muscle loss in the quadriceps femoris. *J Biomech.* 2014;47(9):2013-2021.
  12. Corona BT, Rivera JC, Owens JG, Wenke JC, Rathbone CR. Volumetric Muscle Loss Leads To Permanent Disability Following Extremity Trauma. *J Rehabil Res Dev.* 2015;52:785-792. In Press.
  13. Papakostidis C, Kanakaris NK, Pretel J, Faour O, Morell DJ, Giannoudis PV. Prevalence of complications of open tibial shaft fractures stratified as per the Gustilo-Anderson classification. *Injury.* 2011;42(12):1408-1415.
  14. Hurtgen BJ, Ward CL, Garg K, et al. Severe muscle trauma triggers heightened and prolonged local musculoskeletal inflammation and impairs adjacent tibia fracture healing. *J Musculoskelet Neuronal Interact.* 2016;16(2):122-134.
  15. Hamrick MW. A role for myokines in muscle-bone interactions. *Exerc Sport Sci Rev.* 2011;39(1):43-47.
  16. Hamrick MW, McNeil PL, Patterson SL. Role of muscle-derived growth factors in bone formation. *J Musculoskelet Neuronal Interact.* 2010;10(1):64-70.
  17. Harry LE, Sandison A, Paleolog EM, Hansen U, Pearse MF, Nanchahal J. Comparison of the healing of open tibial fractures covered with either muscle or fasciocutaneous tissue in a murine model. *J Orthop Res.* 2008;26(9):1238-1244.
  18. Kaufman H, Reznick A, Stein H, Barak M, Maor G. The biological basis of the bone-muscle inter-relationship in the algorithm of fracture healing. *Orthopedics.* 2008;31(8):751.
  19. Haas GJ, Dunn AJ, Marcinczyk M, et al. Biomimetic sponges for regeneration of skeletal muscle following trauma. *J Biomed Mater Res A.* 2019;107(1):92-103.
  20. Haas G, Dunn A, Madsen J, et al. Biomimetic sponges improve muscle structure and function following volumetric muscle loss. *bioRxiv.* 2020:2020.05.20.106823.
  21. Corona BT, Garg K, Ward CL, McDaniel JS, Walters TJ, Rathbone CR. Autologous minced muscle grafts: a tissue engineering therapy for the volumetric loss of skeletal muscle. *Am J Physiol Cell Physiol.* 2013;305(7):C761-C775.
  22. Garg K, Corona BT, Walters TJ. Losartan administration reduces fibrosis but hinders functional recovery after volumetric muscle loss injury. *J Appl Physiol.* 2014;117(10):1120-1131.
  23. Garg K, Ward CL, Rathbone CR, Corona BT. Transplantation of devitalized muscle scaffolds is insufficient for appreciable *de novo* muscle fiber regeneration after volumetric muscle loss injury. *Cell Tissue Res.* 2014;358(3):857-873.
  24. Mehta M, Strube P, Peters A, et al. Influences of age and mechanical stability on volume, microstructure, and mineralization of the fracture callus during bone healing: is osteoclast activity the key to age-related impaired healing? *Bone.* 2010;47(2):219-228.
  25. Hurtgen BJ, Henderson BEP, Ward CL, et al. Impairment of early fracture healing by skeletal muscle trauma is restored by FK506. *BMC Musculoskelet Disord.* 2017;18(1):253-253.
  26. Willett NJ, Li MT, Uhrig BA, et al. Attenuated human bone morphogenetic protein-2-mediated bone regeneration in a rat model of composite bone and muscle injury. *Tissue Eng Part C Methods.* 2013;19(4):316-325.
  27. Ruehle MA, Li MA, Cheng A, Krishnan L, Willett NJ, Guldberg RE. Decorin-supplemented collagen hydrogels for the co-delivery of bone morphogenetic protein-2 and microvascular fragments to a composite bone-muscle injury model with impaired vascularization. *Acta Biomater.* 2019;93:210-221.
  28. Ruehle MA, Krishnan L, Vantucci CE, et al. Effects of BMP-2 dose and delivery of microvascular fragments on healing of bone defects with concomitant volumetric muscle loss. *J Orthop Res.* 2019;37(3):553-561.
  29. Pollot BE, Goldman SM, Wenke JC, Corona BT. Decellularized extracellular matrix repair of volumetric muscle loss injury impairs adjacent bone healing in a rat model of complex musculoskeletal trauma. *J Trauma Acute Care Surg.* 2016;81(5):S184-S190.
  30. Warren GL, O'Farrell L, Summan M, et al. Role of CC chemokines in skeletal muscle functional restoration after injury. *Am J Physiol Cell Physiol.* 2004;286(5):C1031-C1036.
  31. Summan M, McKinstry M, Warren GL, et al. Inflammatory mediators and skeletal muscle injury: a DNA microarray analysis. *J Interferon Cytokine Res.* 2003;23(5):237-245.
  32. Peterson JM, Pizza FX. Cytokines derived from cultured skeletal muscle cells after mechanical strain promote neutrophil chemotaxis *in vitro.* *J Appl Physiol.* 2009;106(1):130-137. (1985).
  33. Crescioli C, Sottili M, Bonini P, et al. Inflammatory response in human skeletal muscle cells: CXCL10 as a potential therapeutic target. *Eur J Cell Biol.* 2012;91(2):139-149.
  34. Ishiuchi Y, Sato H, Tsujimura K, et al. Skeletal muscle cell contraction reduces a novel myokine, chemokine (C-X-C motif) ligand 10 (CXCL10): potential roles in exercise-regulated angiogenesis. *Biosci Biotechnol Biochem.* 2018;82(1):97-105.
  35. Kim J, Choi JY, Park SH, et al. Therapeutic effect of anti-C-X-C motif chemokine 10 (CXCL10) antibody on C protein-induced myositis mouse. *Arthritis Res Ther.* 2014;16(3):R126.
  36. Tiefenthaler M, Hofer S, Ebner S, et al. In vitro treatment of dendritic cells with tacrolimus: impaired T-cell activation and IP-10 expression. *Nephrol Dial Transplant.* 2004;19(3):553-560.
  37. Cai D, Frantz JD, Tawa NE, Jr., et al. IKKbeta/NF-kappaB activation causes severe muscle wasting in mice. *Cell.* 2004;119(2):285-298.
  38. Hunter RB, Kandarian SC. Disruption of either the Nfkb1 or the Bcl3 gene inhibits skeletal muscle atrophy. *J Clin Invest.* 2004;114(10):1504-1511.
  39. Hunter RB, Stevenson E, Koncarevic A, Mitchell-Felton H, Essig DA, Kandarian SC. Activation of an alternative NF-kappaB pathway in skeletal muscle during disuse atrophy. *FASEB J.* 2002;16(6):529-538.

40. Deyhle MR, Hyldahl RD. The role of T lymphocytes in skeletal muscle repair from traumatic and contraction-induced injury. *Front Physiol.* 2018;9:768.
41. Skrenta H, Yang Y, Pestka S, Fathman CG. Ligand-independent down-regulation of IFN-gamma receptor 1 following TCR engagement. *J Immunol.* 2000;164(7):3506-3511.
42. Toben D, Schroeder I, El Khassawna T, et al. Fracture healing is accelerated in the absence of the adaptive immune system. *J Bone Miner Res.* 2011;26(1):113-124.
43. Schmidt-Bleek K, Schell H, Schulz N, et al. Inflammatory phase of bone healing initiates the regenerative healing cascade. *Cell Tissue Res.* 2012;347(3):567-573.
44. Shefelbine SJ, Augat P, Claes L, Beck A. Intact fibula improves fracture healing in a rat tibia osteotomy model. *J Orthop Res.* 2005; 23(2):489-493.
45. Villafan-Bernal JR, Franco-De La Torre L, Sandoval-Rodriguez AS, et al. Molecular profiling of a simple rat model of open tibial

fractures with hematoma and periosteum disruption. *Exp Ther Med.* 2016;12(5):3261-3267.

#### SUPPORTING INFORMATION

Additional Supporting Information may be found online in the supporting information tab for this article.

**How to cite this article:** Dunn A, Haas G, Madsen J, et al. Biomimetic sponges improve functional muscle recovery following composite trauma. *J Orthop Res.* 2022;40: 1039-1052. <https://doi.org/10.1002/jor.25143>